Journal of Computational Physics **164,** 204–227 (2000)
doi:10.1006/jcph.2000.6600, available online at http://www.idealibrary.com on IDEAL®

Adjoint Error Estimation and Grid Adaptation for Functional Outputs: Application to Quasi-One-Dimensional Flow

David A. Venditti and David L. Darmofal

Department of Aeronautics and Astronautics, Massachusetts Institute of Technology, 77 Massachusetts Avenue, Room 37-442, Cambridge, Massachusetts 02139
E-mail: venditti@mit.edu

Received December 16, 1999; revised July 12, 2000

An error estimation and grid adaptive strategy is presented for estimating and reducing simulation errors in functional outputs of partial differential equations. The procedure is based on an adjoint formulation in which the estimated error in the functional can be directly related to the local residual errors of both the primal and adjoint solutions. This relationship allows local error contributions to be used as indicators in a grid-adaptive strategy designed to produce specially tuned grids for accurately estimating the chosen functional. In this paper, attention is limited to one-dimensional problems, although the procedure is readily extendable to multiple dimensions. The error estimation procedure is applied to a standard, second-order, finite volume discretization of the quasi-one-dimensional Euler equations. Both isentropic and shocked flows are considered. The chosen functional of interest is the integrated pressure along a variable-area duct. The error estimation procedure, applied on uniform grids, provides superconvergent values of the corrected functional. Results demonstrate that additional improvements in the accuracy of the functional can be achieved by applying the proposed adaptive strategy to an initially uniform grid. The proposed adaptive strategy is also compared with a standard adaptive scheme based on the interpolation error in the computed pressure. The proposed scheme consistently yields more accurate functional predictions than does the standard scheme.

Key Words: grid adaptation; error estimation; adjoint; functional output.

1. INTRODUCTION

The use of computational simulations in the prediction of complex aerodynamic flows is becoming increasingly prevalent in the design process within the aerospace industry. Continuing advancements in both computing technology and algorithmic development are

0021-9991/00 $35.00

ultimately leading to attempts at simulating ever-larger, more complex problems. The efficiency of the underlying computational algorithms is critical and is often the limiting factor in the applicability of computational fluid dynamics as a viable analysis tool in design. Among the difficulties associated with increased problem complexity are the large number of degrees of freedom required to accurately predict the flow field.

A well-known strategy for minimizing the required mesh size for a given level of accuracy is grid adaptation [3, 5, 10, 16, 18, 26–29]. The basic premise is to locally enrich the grid in regions which most adversely affect the accuracy of the final solution while coarsening the grid in more benign regions to prevent incurring unnecessary computational costs. A major difficulty in achieving definite improvements using adaptation for Euler and Navier–Stokes calculations is the lack of a reliable error indicator. A common strategy is to adapt to certain physical features of the flow, such as shock waves, slip lines, or stagnation points, by employing indicators based on large flow gradients [3, 27]. This approach is quite straightforward to implement since the indicators can be computed directly from the evolving flow field, which is readily available. However, continuous local refinement of the dominant flow features does not necessarily guarantee that certain measures of the global error will simultaneously be reduced. In certain cases this procedure may even lead to incorrect results [27]. Another strategy is to develop adaptive criteria based on *a posteriori* error estimates [1, 4, 5, 8, 10, 13, 14, 17, 19, 26, 28–30]. A common approach [10, 28, 29] has been to use local gradient recovery techniques to obtain higher order projections of the solution gradients. The solution is then compared with the higher order projection to assess the error. For elliptic problems and, in particular, finite element methods, this procedure provides rigorous error estimates based on particular norms of the solution and its derivatives. Unfortunately, for convection-dominated problems, such as those encountered in aerodynamic applications, these error estimates can no longer be made rigorous. In addition, even within the setting of finite-element-discretized, elliptic problems, one can argue that a global error norm based directly on the solution and its derivatives may not be optimal within an engineering context.

An alternate approach to making error estimation more relevant to engineering applications is to assess the error made in predicting an integral quantity representing an engineering output. For example, in aerodynamic applications, this output might be the lift or drag. To this end, procedures have been outlined by Rannacher and collaborators [4, 5, 13], Pierce and Giles [19], Machiels *et al.* [14], and Venditti and Darmofal [26]. They are based on concepts already known from structural finite element methods [2]. These procedures invoke the concept of duality, in which an equivalent dual (adjoint) formulation of the primal problem is exploited. The primary benefit of invoking the dual problem, in the context of error estimation, is that the error in a chosen functional can be directly related to local residual errors of the primal solution through the adjoint variables. More precisely, the error can be expressed as an inner product of the local residual errors and the adjoint variables. This property elucidates the potential for devising optimal grid adaptive strategies designed to produce specially tuned grids for maximizing the accuracy of a particular functional.

There are two common approaches to formulating the dual problem: the *continuous* approach and the *discrete* approach. In the continuous approach an objective function is formed by augmenting the functional of interest with Lagrange multipliers (adjoint variables) to enforce the flow constraints (the original primal, nonlinear, partial differential equations). The next step is to consider linear perturbations to the primal flow variables and to require that the objective function remains stationary with respect to these perturbations.

The analytical adjoint equations are forthwith obtained, together with appropriate boundary conditions, and are then discretized directly. One benefit to the continuous approach is that it more readily offers insight into the nature of the adjoint solution [9]. In the discrete approach one begins with the nonlinear, discrete residual equations associated with the primal problem and then considers linear perturbations to these. The resulting linear system of equations also yields a consistent approximation of the adjoint solution. A convenience associated with the discrete approach is that the adjoint equations and corresponding boundary conditions need not be derived and discretized explicitly. All that is needed are the linear sensitivities of the functional and the Jacobian matrix associated with the primal residual. The adjoint boundary conditions are automatically incorporated into the formulation via the primal residual operator. Many existing Euler and Navier–Stokes codes (especially those that employ adjoint-based optimization algorithms [6, 12, 15]) already have much of the machinery that would be required to implement an adjoint error estimation/grid adaptation procedure such as the one described in this paper.

The main contributions of this paper are summarized in the following. A new methodology is presented which uses the discrete adjoint solution to relate local errors in the flow solution to the global error in the functional of interest. The method of Pierce and Giles [19] also uses the adjoint solution for this purpose; however, their approach uses an analytic viewpoint whereas the current formulation is cast in a discrete framework. The two approaches are closely related under certain conditions that will be elaborated upon in Section 2. A convenience associated with the current approach is that the error contribution from the domain boundary is automatically incorporated into the expression for the computable error estimate. In the method of Pierce and Giles, additional error terms may be required to account for inhomogeneous boundary conditions [19]. There are also advantages and disadvantages associated with the ease of implementation of the two approaches. This will also be addressed in Section 2. Both the current approach and the method of Pierce and Giles have the advantage of being applicable to general discretizations, whereas other procedures are implicitly linked to a particular discretization such as the finite element method [4, 5, 13, 14, 17]. Another contribution presented in this paper is the use of adjoint error analysis to derive criteria for driving a grid-adaptive process. Our intention is to further improve the accuracy of the predicted functional by coupling the aforementioned error estimation procedure with an adjoint-based grid-adaptive strategy. The adaptive strategy incorporates the novel use of a *duality gap*, which, among other things, quantifies certain nonlinear contributions to the global error in the functional.

The organization of the paper is as follows: First, the proposed error estimation procedure is outlined. In the first stage of the procedure, we strive to estimate the value of a functional on a fine grid without actually solving on this grid. The only auxiliary computations required to calculate this estimate are functional and residual evaluations on the fine grid and the solution of a linear adjoint problem on a coarse grid. The second stage of the estimation procedure involves estimating the exact value of the functional using multiple fine-grid estimates in a multilevel extrapolation process. The error estimation procedure is tested on a finite volume discretization of the quasi-one-dimensional Euler equations on uniform grids. Results are presented for three test cases: subsonic flow, isentropic transonic flow, and shocked transonic flow through a converging–diverging duct. The functional of interest in each case is the integrated pressure along the duct. Next, we proceed to outline the adaptive methodology. The primary objective of the proposed adaptive strategy is to improve the accuracy of the aforementioned error estimation procedure to obtain a more accurate functional after

correction. This is in contrast to other adaptive strategies that are designed to improve the accuracy of the computed functional directly. Robustness of the iterative adaptive procedure is also of concern in our choice of adaptive criteria. Finally, one-dimensional adaptive results are presented and demonstrate that further improvements in the overall accuracy of the computed functional can be achieved using the proposed adaptive strategy in conjunction with the error estimation procedure. The proposed adaptive strategy is also compared with a standard adaptive scheme driven by a measure of the interpolation error in the computed pressure [3, 27]. Adaptive results using the proposed scheme are consistently more accurate than those of the standard scheme.

2. ERROR ESTIMATION PROCEDURE

Consider the coarse mesh Ω_H as being an affordable mesh with respect to available computing resources and allowable solution times. The parameter H represents a characteristic length associated with the discretization such as the cell spacing in a finite volume scheme or the average element size in a finite element scheme. We are interested in estimating an integral quantity $f(U)$, where U is the solution of the system of partial differential equations (PDEs) under consideration. The approximation of this integral on Ω_H using a prescribed quadrature rule is denoted by $f_H(U_H)$, where U_H is the corresponding discrete solution on Ω_H.

Although $f_H(U_H)$ can be computed affordably, it may not be sufficiently accurate for the intended application. Now consider a fine mesh Ω_h as being a mesh that is too expensive for the purposes of estimating $f(U)$; however, if a discrete solution U_h were obtained on Ω_h, the corresponding discrete integral $f_h(U_h)$ would be sufficiently accurate for our purposes. We further require that Ω_h be embedded within Ω_H. In other words, Ω_h is constructed, locally, by subdividing each of the elements of Ω_H into an integer number n of self-similar[1] subelements, where $n = (H/h)^d$ and d is the number of spatial dimensions in the problem.

Our goal is to obtain an accurate estimate of $f_h(U_h)$ without ever solving on the fine mesh Ω_h. The point of departure in this analysis is a multiple variable Taylor series expansion of $f_h(U_h)$ about the coarse mesh solution,

$$f_h(U_h) = f_h\left(U_h^H\right) + \left.\frac{\partial f_h}{\partial U_h}\right|_{U_h^H}\left(U_h - U_h^H\right) + \cdots. \tag{1}$$

The column vector U_h^H represents the coarse mesh solution mapped onto the fine mesh Ω_h via some prolongation operator. The row vector $\partial f_h/\partial U_h|_{U_h^H}$ contains the linear sensitivities of the fine-mesh functional evaluated using U_h^H. Introducing the prolongation operator I_h^H, we can write the vector U_h^H as

$$U_h^H \equiv I_h^H U_H. \tag{2}$$

The prolongation operator I_h^H interpolates or reconstructs the coarse-mesh solution and maps it onto the fine mesh. The order of the prolongation should be greater than, or at least consistent with, the order of the discretization. An appropriate definition for I_h^H could

[1] The requirement of self-similarity of sub-elements will need to be relaxed for certain types of grids as will be discussed below.

depend on the underlying discretization method and on the classification (elliptic or hyperbolic) of the PDE(s) being approximated. In the case of a finite difference discretization, I_h^H could represent higher order interpolation through the computed nodal values of the coarse-mesh solution. In the case of a finite element discretization I_h^H could represent injection from the coarse-mesh basis functions directly or from a higher order projection of the finite element solution [19]. If the PDEs have a hyperbolic character to them, isodirectional interpolation might lead to oscillatory behavior in an iterative adaptive procedure, as was initially encountered in the current implementation of the proposed adaptive strategy. Alternative reconstruction approaches may be required to overcome this difficulty. This is discussed further in Section 4.2.

The nonlinear residual operator representing the system of equations arising from some discretization of the original partial differential equations on the fine mesh is denoted by

$$R_h(U_h) = 0. \tag{3}$$

Linearizing about the coarse-mesh solution yields

$$R_h(U_h) = R_h\left(U_h^H\right) + \left.\frac{\partial R_h}{\partial U_h}\right|_{U_h^H}\left(U_h - U_h^H\right) + \cdots, \tag{4}$$

where $\partial R_h/\partial U_h|_{U_h^H}$ is the Jacobian of the fine-mesh system of equations evaluated using U_h^H. Symbolically, we can invert (4) to obtain an approximation of the error vector (that is, the coarse-mesh-solution error measured with respect to the fine-mesh solution)

$$\left(U_h - U_h^H\right) \approx -\left[\left.\frac{\partial R_h}{\partial U_h}\right|_{U_h^H}\right]^{-1} R_h\left(U_h^H\right). \tag{5}$$

Substituting (5) into (1) gives

$$f_h(U_h) \approx f_h\left(U_h^H\right) - \left(\Psi_h|_{U_h^H}\right)^T R_h\left(U_h^H\right), \tag{6}$$

where $\Psi_h|_{U_h^H}$ is the discrete adjoint solution satisfying

$$\left[\left.\frac{\partial R_h}{\partial U_h}\right|_{U_h^H}\right]^T \Psi_h|_{U_h^H} = \left(\left.\frac{\partial f_h}{\partial U_h}\right|_{U_h^H}\right)^T. \tag{7}$$

Equation (6) is an estimate of $f_h(U_h)$. It is exact for linear residuals and functionals. To compute this estimate would require the solution of the adjoint problem on the fine mesh, which is undesirable. Instead, $\Psi_h|_{U_h^H}$ is replaced by the interpolated coarse-mesh adjoint $L_h^H\Psi_H$, where L_h^H is a prolongation operator which expresses the coarse-mesh adjoint on the fine mesh by interpolation. Utilizing L_h^H, and the reconstruction operator I_h^H, in (6) yields the final, computable estimate as

$$\tilde{f}_h(U_H) = f_h\left(I_h^H U_H\right) - \left(L_h^H\Psi_H\right)^T R_h\left(I_h^H U_H\right), \tag{8}$$

where Ψ_H is obtained from the solution of the discrete adjoint equations on the coarse grid:

$$\left[\frac{\partial R_H}{\partial U_H}\right]^T \Psi_H = \left(\frac{\partial f_H}{\partial U_H}\right)^T. \tag{9}$$

The coarse grid Ω_H should be fine enough to capture the essential features of the problem under consideration (that is, the corresponding discrete solution U_H should be within the asymptotic range) in order for the truncated expansions, (1) and (4), to be uniformly valid. In practice, however, decent error estimates have been obtained on fairly coarse grids, as will be demonstrated in Section 3.4 when the numerical results are presented.

We now describe a method of estimating the exact value of the functional $f(U)$. This is achieved by utilizing two or more fine meshes in a multilevel error estimation procedure similar to Richardson extrapolation [20]. A key distinction from Richardson extrapolation is that the current approach extrapolates error estimates as opposed to extrapolating discrete solutions computed on grids of different spacing. Thus, only one coarse grid solution is required to apply this procedure. Furthermore, it is not restricted to uniform base-grids. Strictly, one could interpret the current procedure as a particular application of Richardson's deferred approach to the limit [21].

Let p be the observed rate of convergence of the error in the coarse-grid functional. We define a series of fine meshes Ω_{h_i}, $i = 1, 2, \ldots, m$, such that the corresponding characteristic cell or element sizes satisfy $h_i > h_{i+1}$. Furthermore, the ith mesh Ω_{h_i} is constructed by subdividing each of the elements of Ω_H into an integer number n_i of self-similar subelements, where $n_i = (H/h_i)^d$. The discrete functional on the ith fine mesh can be estimated using (8). This estimate is denoted here by $\tilde{f}_{h_i}$. The multilevel procedure is based on the observation that the true error in the estimated functional, $\tilde{f}_{h_i} - f(U)$, computed from a smooth base solution, converges like h_i^p. This may also be true for certain integral quantities computed from discontinuous base-solutions including shocked flows [7]. Considering two different fine meshes, $i = 1$ and $i = 2$, we may, therefore, write

$$\begin{aligned} \tilde{f}_{h_1} - f(U) &= ch_1^p + O\left(h_1^{p+1}\right), \\ \tilde{f}_{h_2} - f(U) &= ch_2^p + O\left(h_2^{p+1}\right). \end{aligned} \tag{10}$$

Neglecting the higher order terms, eliminating c, and solving for $f(U)$ yields the $O(h^{p+1})$ estimate as

$$f(U) \approx \frac{\tilde{f}_{h_1} h_2^p - \tilde{f}_{h_2} h_1^p}{h_2^p - h_1^p}. \tag{11}$$

Convergence rates even better than $O(h^{p+1})$ have been observed for the test cases considered in this paper using the current estimation scheme.

It should be noted that constructing a hierarchy of fine grids in the manner suggested above may not be possible for certain types of grids. For example, one cannot subdivide a tetrahedron into self-similar tetrahedra. In such cases, the condition of self-similarity of the subelements would have to be relaxed. One alternative approach, in the case of a tetrahedral base-mesh, would be to first choose a systematic method of discretizing a single, arbitrary tetrahedron into subtetrahedra. For example, a 1 : 12 refinement ratio could be achieved by adding nodes to the midpoints of each of the edges of the original tetrahedron and by adding one more node to its centroid. The application of this systematic refinement algorithm to each tetrahedron in the base-mesh would thereby define an embedded fine mesh. Recursive repetition of this procedure would result in a hierarchy of grids where each successive grid would be embedded within the previous one.

We now briefly mention some differences between the proposed error estimation procedure and the adjoint-based correction method of Pierce and Giles [19]. The current

formulation is cast in a discrete framework whereas their approach uses an analytic viewpoint. The two methods become closely related as the fine grid Ω_h in the current procedure becomes infinitely resolved (that is, as $h \to 0$). A convenience associated with the current approach is that the error contribution from the domain boundary is automatically accounted for in the error estimate given by (8). This is due to the fact that the boundary conditions are already incorporated into the residual operator in the current formulation. In the method of Pierce and Giles, additional error terms may be required to account for inhomogeneous boundary conditions [19]. With regard to the quality of the resulting error estimates, both approaches appear to give similar accuracy; however, additional work would be required to verify this.

Finally, we address the issue of implementing the proposed procedure into an existing flow solver. Depending on the structure of the source code, it could be possible to implement the current procedure very rapidly into a flow solver that already computes the adjoint solution (such as an adjoint-based, aerodynamic optimization code [6, 12, 15]), especially if the residual and functional operators are readily available. However, a naive implementation of the procedure would entail storing at least one embedded fine grid in its entirety in order to avoid modifying the machinery of the code. This could become prohibitive in multiple dimensions. A memory-efficient implementation would necessitate more coding work to avoid storing an entire fine grid in memory. Thus the advantage of an easy implementation would be lost unless memory were not an issue.

3. UNIFORM GRID RESULTS

The error estimation strategy outlined in the previous section is tested on the quasi-1D Euler equations using a standard second-order finite volume scheme on uniformly spaced grids.

3.1. *Quasi-1D Euler Equations*

The quasi-1D Euler equations describe the flow of an inviscid, compressible, ideal gas through thin variable-area ducts [11, 23]. The steady-state equations may be written in the form

$$\frac{dF(U)}{dx} = J(U), \tag{12}$$

where U, F, and J are given by

$$U = \begin{Bmatrix} \rho A \\ \rho V A \\ \rho E A \end{Bmatrix}, \quad F = \begin{Bmatrix} \rho V A \\ (\rho V^2 + p)A \\ \rho V \bar{h}_o A \end{Bmatrix}, \quad J = \begin{Bmatrix} 0 \\ p(dA/dx) \\ 0 \end{Bmatrix}. \tag{13}$$

In these expressions, ρ is the mass density, V is the gas velocity, p is the static pressure, E is the total energy, $\bar{h}_o = E + p/\rho$ is the stagnation enthalpy, and $A(x)$ is the cross-sectional area of the duct. The system is closed with the equation of state for an ideal gas:

$$p = \rho(\gamma - 1)\left(E - \frac{V^2}{2}\right), \tag{14}$$

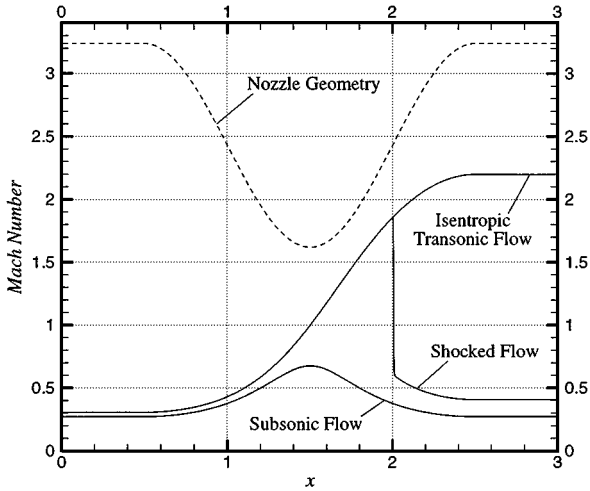

FIG. 1. Nozzle geometry and computed Mach number distributions for the quasi-1D Euler test cases considered.

where γ is the ratio of specific heats. Three different test cases are considered: subsonic flow, isentropic transonic flow, and shocked transonic flow through a converging–diverging nozzle. These flows are depicted in Fig. 1 in terms of the Mach number M, where $M \equiv V/c$ and $c = \sqrt{\gamma p/\rho}$ is the local speed of sound. The nozzle geometry, also shown in Fig. 1, is symmetric about the throat location, with a length of $L = 3$ and a throat-to-exit area ratio of $1:2$.

3.2. *Finite Volume Scheme*

Solutions are obtained using a Newton–Raphson iterative technique applied to a cell-centered finite volume scheme. Numerical fluxes are evaluated using Roe's approximate Riemann solver [22]. Second-order accuracy is achieved using variable extrapolation [25] in conjunction with the van Albada limiter [24].

3.3. *Functional of Interest*

The functional of interest is chosen to be the integral of the pressure p over the domain:

$$f(U) = \int_0^L p\, dx. \tag{15}$$

This functional serves as an analogue for the lift in airfoil or aircraft computations [19]. The pressure distributions for each of the flow regimes considered are plotted in Fig. 2. The discrete functional on all grids is computed using the two-point Newton–Côtes quadrature (Trapezoidal Rule integration). The computed adjoint variables corresponding to the chosen functional are plotted in Fig. 3. There are three adjoint variables, Ψ_1, Ψ_2, and Ψ_3, corresponding to the three conservation equations defined in (12) and (13). It is interesting to note that a logarithmic singularity exists in the adjoint variables at the sonic throat for both the isentropic transonic and shocked flow cases. Their presence reflects the fact that the value of the integrated pressure is infinitely sensitive to a linear perturbation

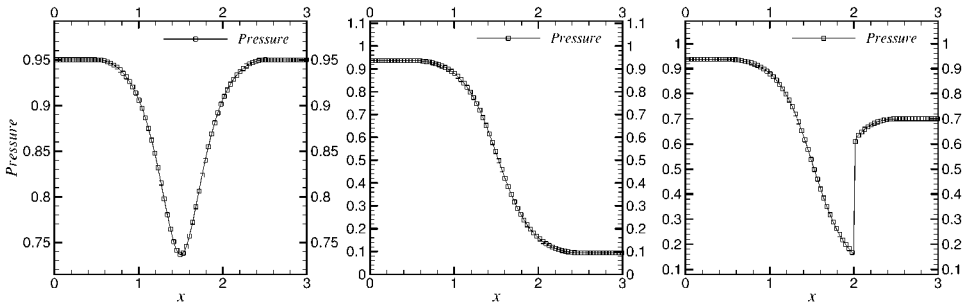

FIG. 2. Computed pressure distributions along the nozzle for each of the quasi-1D Euler test cases considered. Left: subsonic flow; center: isentropic transonic flow; right: shocked flow.

in the flow variables at the choked throat. These singularities were observed by Giles and Pierce [9] in an analytical investigation of the properties of the continuous adjoint equations. Fortunately, the singularities have not resulted in a degradation of the error estimates, as will be demonstrated below. It is also interesting to note that the adjoint variables are continuous across the shock and have zero gradient there [9].

3.4. *Numerical Results*

The error estimation procedure requires that an appropriate reconstruction operator I_h^H be defined to compute (8). The reconstruction operator must accurately represent the coarse-grid solution at the embedded fine-grid cell centers. To achieve this, the coarse-grid solution is assumed to vary over each coarse-grid cell in accordance with the variable extrapolation and limiting procedure used in the finite volume scheme. The coarse-grid solution at the center of an embedded fine-grid cell is obtained by direct injection from this limited, higher order reconstruction over the associated coarse-grid cell. While this method of reconstruction works well for the error estimation procedure, it results in oscillatory behavior in the iterative adaptive procedure to be outlined in the next section. Alternative reconstructions which take into account the hyperbolic character of the flow equations were implemented and led to reductions in the oscillations; however, they came at the cost of reductions in the accuracy of the error estimates, in general. To maintain the quality of the error estimates, we chose, instead, to control the oscillations using a local least squares smoothing technique

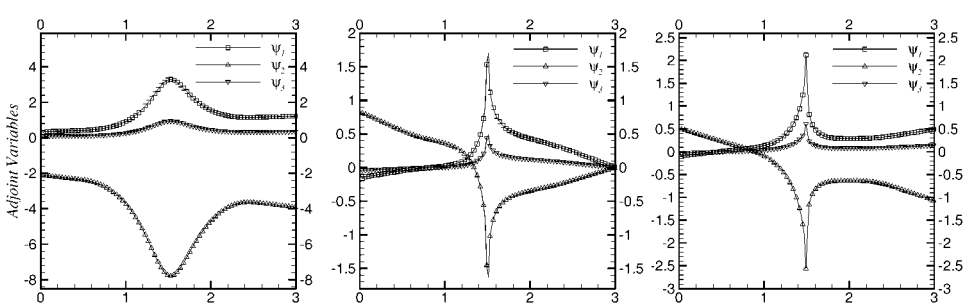

FIG. 3. Computed adjoint flow solutions corresponding to the integrated pressure along the nozzle for each of the quasi-1D Euler test cases considered. Left: subsonic flow; center: isentropic transonic flow; right: shocked flow.

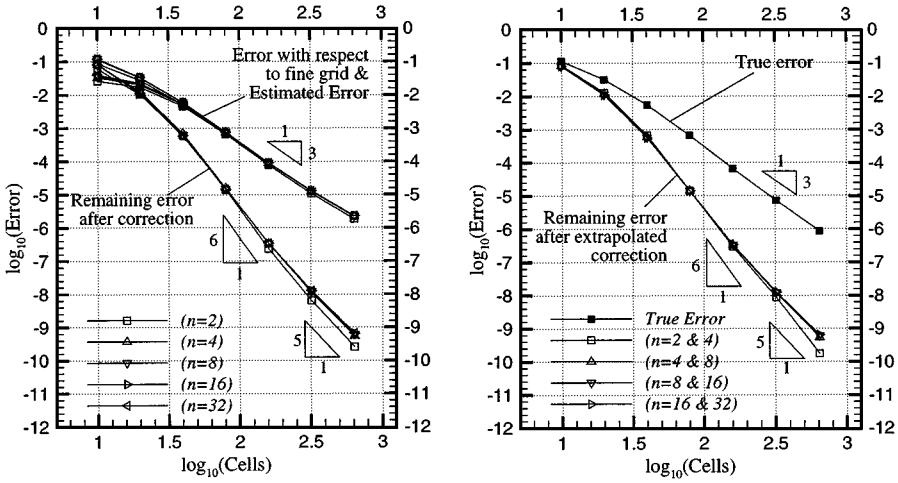

FIG. 4. Error convergence plots on uniform grids for the subsonic test case. In the left plot, errors are measured with respect to finer grid values of the functional. In the right plot, errors are measured with respect to the exact (analytical) value of the functional ($f(U) \approx 2.707$).

and to retain the aforementioned limited, higher order reconstruction as the definition of I_h^H for all the test cases in this paper.

The prolongation operator L_h^H, used to express the coarse-grid adjoint onto the fine grid, was chosen as quadratic interpolation through adjacent coarse-grid cell centers. Linear interpolation also yields the same asymptotic convergence rates as quadratic interpolation with only a slight degradation in the quality of the corresponding error estimates. The choice of quadratic interpolation over linear interpolation was, therefore, quite arbitrary for the quasi-1D test cases and functional considered in this paper. It should be noted, however, that for multidimensional problems and/or problems involving boundary-integral functionals, the order of the prolongation operator should be greater than the order of the corresponding discretization to ensure that the superconvergent property of the error estimates is preserved [26].

A series of error convergence plots corresponding to the subsonic, isentropic transonic, and shocked flow cases are presented in Figs. 4, 5, and 6, respectively. In each of these plots a measure of the error in the coarse-grid functional is plotted versus the total number of cells in the corresponding coarse grid. These errors are absolute errors plotted on a logarithmic scale. The functional values are $f(U) \approx 2.707$, 1.558, and 2.138 for the subsonic, isentropic transonic, and shocked flow cases, respectively. A total of seven different uniformly spaced coarse grids are considered in these plots ranging from 10 to 640 cells. For each of these coarse grids five different fine grids are constructed corresponding to $n = 2$, 4, 8, 16, and 32. The fine-grid sizes, therefore, range from 20 to 20,480 cells. In the left-most plots of Figs. 4, 5, and 6, the functional error is measured with respect to the fine-grid values of the functional.[2] The error, $|f_h(I_h^H U_H) - f_h(U_h)|$, estimated error, $|(L_h^H \Psi_H)^T R_h(I_h^H U_H)|$, and the remaining error after correction, $|f_h(I_h^H U_H) - f_h(U_h) - (L_h^H \Psi_H)^T R_h(I_h^H U_H)|$,

[2] Solutions were obtained on each fine grid for the purposes of computing the corresponding functional errors needed for the convergence plots. It is reiterated here that the error estimation procedure, itself, does not require solutions on the fine grids.

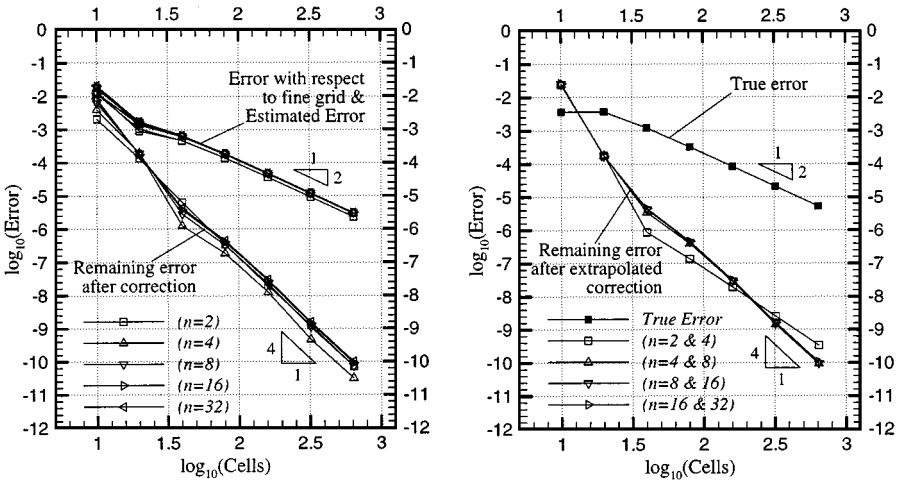

FIG. 5. Error convergence plots on uniform grids for the isentropic transonic test case. In the left plot, errors are measured with respect to finer grid values of the functional. In the right plot, errors are measured with respect to the exact (analytical) value of the functional ($f(U) \approx 1.558$).

are plotted for each of the flow regimes considered. In the right plot of each figure, the functional error is measured with respect to the exact, analytical value of the functional. We refer to this error as the *true error*, which is given by $|f_H(U_H) - f(U)|$. The estimated true error is obtained using (11). As before, the remaining errors after correction are also shown in the plots on the right.

The error in the functional exhibits $O(h^3)$ (asymptotic) convergence in the subsonic test case and $O(h^2)$ convergence in the transonic test cases. After applying the error estimation/correction procedure to the coarse-grid functionals we obtain a doubling in the accuracy to approximately $O(h^6)$ convergence and $O(h^4)$ convergence in the subsonic and transonic

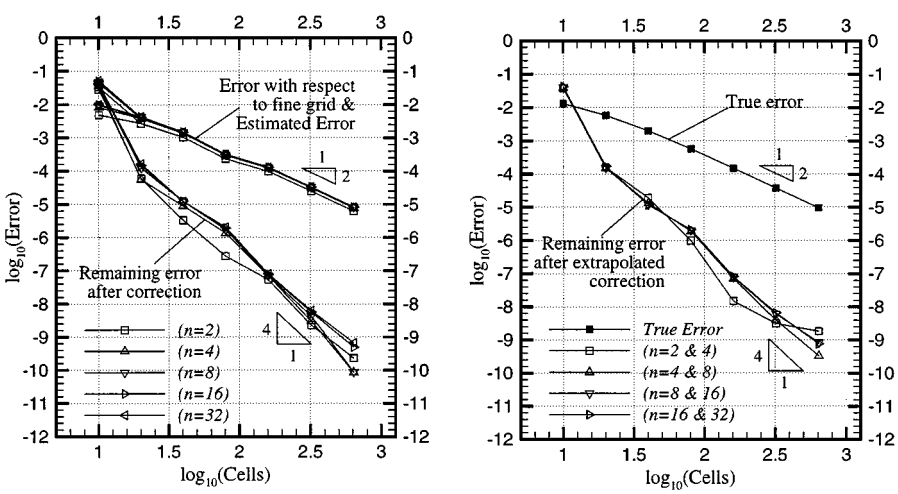

FIG. 6. Error convergence plots on uniform grids for the shocked test case. In the left plot, errors are measured with respect to finer grid values of the functional. In the right plot, errors are measured with respect to the exact (analytical) value of the functional ($f(U) \approx 2.138$).

test cases, respectively. The lower order error convergence in the isentropic transonic test case is likely due to the singularity in the adjoint variables at the throat (see Fig. 3). In the shocked case, both the adjoint singularity and primal discontinuity are likely contributors to the lower order convergence in the functional error as compared to the subsonic case. It should be noted that the error estimates are relatively independent of the values of n for each of the test cases considered, as is evident from Figs. 4, 5, and 6.

The solutions on the coarsest of the coarse grids (10 cells) are not within the asymptotic range for these problems. The corresponding error estimates, therefore, are not particularly accurate since they rely, to a certain extent, on the coarse-grid solutions being accurate enough to capture the essential features of the problem. The 20-cell coarse-grid solutions are, at best, barely within the asymptotic range; however, the corresponding error estimates are already providing significant improvements in the accuracy of the functional. On the finest of the coarse grids (1280 cells), the errors in the functionals are being reduced by several orders of magnitude.

Pierce and Giles [19] applied their adjoint-based correction procedure to a series of similar quasi-1D test cases. They also achieved a doubling in the accuracy of the integrated pressure in two isentropic test cases. In a shocked test case, however, the improvement in convergence was only $O(h^2)$ to $O(h^3)$ after correction. The extra order of accuracy obtained for the shocked case in this paper is likely attributable to the discretization method and not to the error estimation procedure per se. This has not been confirmed, however.

The results presented in Figs. 4, 5, and 6 demonstrate that significant improvements in the accuracy of the functional can be obtained in each of the test cases using the proposed error estimation/correction procedure on uniform grids. We now proceed to outline the adaptive strategy and demonstrate that further improvements in the accuracy of the functional can be obtained using the error estimation procedure in conjunction with the proposed adaptive algorithm.

4. GRID ADAPTATION STRATEGY

In this section we propose an adaptive strategy designed to improve the accuracy of the computable error estimate in (8). This is in contrast to other adaptive schemes that attempt to optimize the computational grid with respect to maximizing the accuracy of the base functional directly [5]. One variant of the latter approach could be based exclusively on (8), where it is evident that the error in the functional can be expressed as a weighted sum of the local residual errors with the adjoint variables as the weights. These local error contributions could be used as indicators in a grid adaptive strategy designed to yield near-optimal grids for computing the chosen functional. Unfortunately, this approach could lead to erroneous requests to the grid generator for refinement and/or coarsening in regions where the adjoint solution is not sufficiently resolved. We wish to reduce this risk by deriving more conservative criteria for adaptation based on both the primal and adjoint residual errors. The proposed adaptive strategy involves equidistributing the value of an adaptation parameter throughout the computational domain. We will demonstrate that reducing the proposed adaptation parameter leads to improvements in the quality of the error estimates. In practice, it also leads to improvements in the base value of the functional, before correction. Furthermore, we will show that a fringe benefit of reducing the proposed adaptation parameter is that certain nonlinear contributions to the error are also reduced.

4.1. *Adaptive Criteria*

Let us restrict our attention to a coarse-grid problem and one fine-grid error estimate. To simplify the present discussion, we omit nonlinear effects (a more thorough accounting of the error is presented in the Appendix). Equation (6) can be decomposed in the following manner:

$$f_h\left(U_h^H\right) - f_h(U_h) \approx \underbrace{\left(L_h^H \Psi_H\right)^T R_h\left(U_h^H\right)}_{\text{Computable correction}} + \underbrace{\left(\Psi_h|_{U_h^H} - L_h^H \Psi_H\right)^T R_h\left(U_h^H\right)}_{\text{Error in computable correction}}. \tag{16}$$

The adjoint residual operator R_h^Ψ is defined by

$$R_h^\Psi(\Psi) \equiv \left[\left.\frac{\partial R_h}{\partial U_h}\right|_{U_h^H}\right]^T \Psi - \left(\left.\frac{\partial f_h}{\partial U_h}\right|_{U_h^H}\right)^T. \tag{17}$$

Substituting the coarse-mesh adjoint into the residual operator and noting that $R_h^\Psi(\Psi_h|_{U_h^H}) = 0$ yields

$$R_h^\Psi\left(L_h^H \Psi_H\right) = \left[\left.\frac{\partial R_h}{\partial U_h}\right|_{U_h^H}\right]^T \left(L_h^H \Psi_H - \Psi_h|_{U_h^H}\right). \tag{18}$$

Using this last expression, (16) may be recast as

$$f_h\left(U_h^H\right) - f_h(U_h) \approx \underbrace{\left(L_h^H \Psi_H\right)^T R_h\left(U_h^H\right)}_{\text{Computable correction}} - \underbrace{\left\{R_h^\Psi\left(L_h^H \Psi_H\right)\right\}^T \left[\left.\frac{\partial R_h}{\partial U_h}\right|_{U_h^H}\right]^{-1} R_h\left(U_h^H\right)}_{\text{Error in computable correction}}. \tag{19}$$

Another form of the error in the computable correction (ECC), which is dual to that given in (16), can be obtained using (4) and (19). Specifically,

$$f_h\left(U_h^H\right) - f_h(U_h) \approx \underbrace{\left(L_h^H \Psi_H\right)^T R_h\left(U_h^H\right)}_{\text{Computable correction}} + \underbrace{\left\{R_h^\Psi\left(L_h^H \Psi_H\right)\right\}^T \left(U_h - U_h^H\right)}_{\text{Error in computable correction}}. \tag{20}$$

The proposed adaptive strategy is based on reducing the ECC, thereby improving the accuracy of the computable correction. It is evident from (16), (19), and (20) that the ECC can be written in at least three different forms. According to (19), reducing the local residual errors in both the primal and adjoint solutions simultaneously would lead to a reduction in the ECC. Adapting on both residuals seems advantageous with respect to the robustness of the procedure. In using this form, however, one must address the issue of how to decrease the two residuals simultaneously during the adaptive procedure. In general, the units of the primal and adjoint residuals will be different and their magnitudes could vary significantly. A viable adaptive scheme must ultimately combine the two residuals into a single adaptation parameter for each cell or element in the mesh. For the purposes of adaptation, (16) and (20) provide more convenient forms of the ECC from which to work with. In particular, the ECC can be expressed as the inner product of the adjoint solution error and the primal

residual error (16) or as the inner product of the adjoint residual error and the primal solution error (20). Neglecting nonlinear terms, these two inner products are equal. The magnitudes of their corresponding components are comparable and their units are equal to those of the functional $f(U)$. This illustrates the duality between the primal and adjoint residual operators. If nonlinear effects are accounted for, a duality gap D will exist between the two inner products. By retaining nonlinear terms in (4), one can express the duality gap as

$$\begin{aligned} D &\equiv \left(\Psi_h|_{U_h^H} - L_h^H \Psi_H\right)^T R_h\left(U_h^H\right) - \left\{R_h^\Psi\left(L_h^H \Psi_H\right)\right\}^T \left(U_h - U_h^H\right) \\ &= -\left(\Psi_h|_{U_h^H} - L_h^H \Psi_H\right)^T W, \end{aligned} \tag{21}$$

where W is a vector containing quadratic forms of the primal error. An explicit expression for W is given by Eq. (iii) in the Appendix. The proposed adaptive procedure is based on reducing and/or equidistributing the magnitudes of the components of each of the inner products on the right-hand side of (21). In addition to improving the quality of the computable correction, this will lead to a reduction in the magnitude of the duality gap and hence to a reduction in the nonlinear contribution to the functional error.

There is still the issue of approximating the primal and adjoint solution errors in (21). This will be addressed in the next section.

4.2. *Refinement Strategy*

In the proposed adaptive strategy, we seek to equidistribute the value of an adaptation parameter, ε, over the entire domain. In doing so, our intention is to maximize the quality of the computable error estimate (8), thereby improving the accuracy of the final, corrected functional. For the 1-D test cases in this paper, we attempt to achieve this by repeatedly regenerating the computational grid, in an iterative manner, keeping the total number of cells fixed, until ε takes on a uniform value throughout the domain. While complete remeshing is appropriate for 1-D problems, it may not be practical for multidimensional problems. The proposed criteria for adaptation, however, can be applied to other modes of grid refinement.

Consider the operation of computing an inner product over the fine grid Ω_h embedded within Ω_H. For each coarse-grid cell k, there are n fine-grid cells over which a partial inner product must be computed. For each fine-grid cell $l(k)$, within cell k, there are three subcomponents to the primal and adjoint residual vectors corresponding to the mass, momentum, and energy conservation equations in the quasi-1D flow model. In light of the discussion of the previous section, Eq. (21) suggests the following definition for the adaptation parameter ε_k at cell k:

$$\begin{aligned} \varepsilon_k = \sum_{l(k)} \Big\{ &\left| \left[Q_h^H \Psi_H - L_h^H \Psi_H\right]_{l(k)}^T \left[R_h\left(I_h^H U_H\right)\right]_{l(k)} \right| \\ &+ \left| \left[Q_h^H U_H - I_h^H U_H\right]_{l(k)}^T \left[R_h^\Psi\left(L_h^H \Psi_H\right)\right]_{l(k)} \right| \Big\}. \end{aligned} \tag{22}$$

In this last expression, a term of the form $[V_h]_{l(k)}$, for some generic vector V_h on Ω_h, refers to the 3×1 subvector (component) of V_h corresponding to the fine-grid cell $l(k)$ within the coarse-grid cell k. The summation in (22) is over all fine cells within the kth coarse cell. For the purposes of adaptation, L_h^H and Q_h^H are interpolation operators which map coarse-grid vectors onto the fine grid via linear and quadratic interpolation, respectively. The reconstruction operator I_h^H is defined in Section 3.4.

At each adaptive iteration, a new cell size, $\tilde{H}_k$, is computed from the old one, H_k, according to

$$\tilde{H}_k = \kappa H_k \left(\frac{\bar{\varepsilon}}{\varepsilon_k} \right)^{\omega}, \tag{23}$$

where $\bar{\varepsilon}$ is the root mean square of ε over all coarse grid cells, ω is an underrelaxation factor that ensures monotonic convergence to a final grid in the iterative adaptive procedure, and κ is the constant which, at a particular iteration, allows the new cell sizes to add up to the domain length. In the present computations, a conservative value of $\omega = 0.01$ was used.

If the adaptive procedure were implemented as described above, spurious, high-frequency modes would start to appear in the residual errors after several adaptive iterations. Eventually, these modes would manifest themselves as oscillations in the cell-size distributions. Several attempts were made to overcome this difficulty. The most effective remedy for controlling the oscillations was to use a small number of local least-squares smoothing sweeps on the adaptation parameter at each adaptive iteration prior to computing the new cell-size distribution. The high-frequency modes were effectively annihilated at each iteration before they had a chance to grow. The quality of the error estimates were practically unaffected by this procedure.

4.3. *Numerical Results*

A series of error convergence plots corresponding to the subsonic, isentropic transonic, and shocked flow cases are presented in Figs. 7, 8, and 9, respectively. In each of these plots, uniform and adapted-grid results are compared. Errors are measured with respect to the exact (analytical) value of the functional. Five different grid sizes are considered: 10, 20, 40, 80, and 160 cells. During the adaptive runs, the total number of cells in each grid was kept constant. After the adaptive process was completed for each grid and test

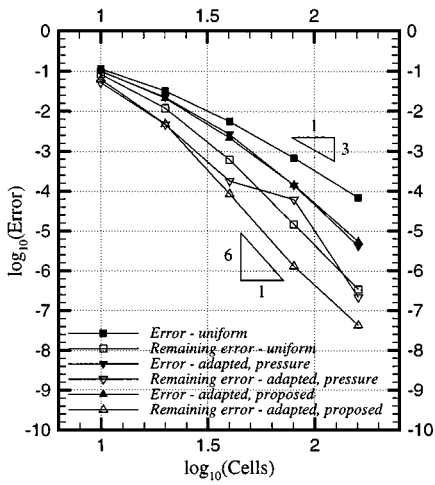

FIG. 7. Error convergence plot on uniform and adapted grids for the subsonic test case. Two sets of adaptive results are presented, one based on equidistributing a measure of the interpolation error in the pressure and the other based on the proposed adaptive criteria. Errors are measured with respect to the exact (analytical) value of the functional ($f(U) \approx 2.707$).

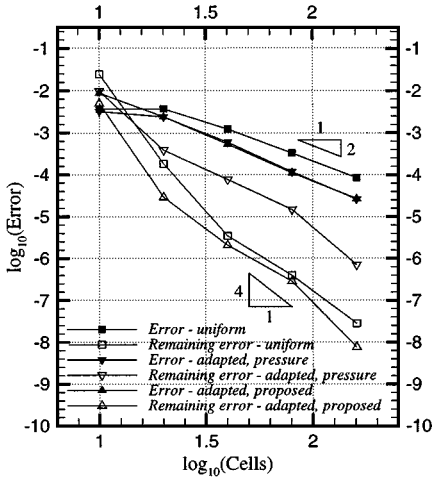

FIG. 8. Error convergence plot on uniform and adapted grids for the isentropic transonic test case. Two sets of adaptive results are presented, one based on equidistributing a measure of the interpolation error in the pressure and the other based on the proposed adaptive criteria. Errors are measured with respect to the exact (analytical) value of the functional ($f(U) \approx 1.558$).

case, the proposed error estimation procedure was applied on the final adapted grid yielding the corrected functional estimates plotted in the figure. Two adaptive criteria were used: the proposed criteria (see Section 4.1) and a standard indicator based on a measure of the interpolation error in the computed pressure [3, 27]. In particular, the standard method strives to equidistribute the value of β over the entire domain, where

$$\beta_k = H_k^2 \left| \frac{\partial^2 p}{\partial x^2} \right|_k \tag{24}$$

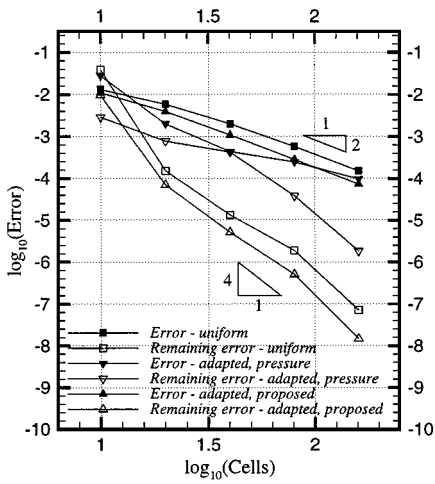

FIG. 9. Error convergence plot on uniform and adapted grids for the shocked test case. Two sets of adaptive results are presented, one based on equidistributing a measure of the interpolation error in the pressure and the other based on the proposed adaptive criteria. Errors are measured with respect to the exact (analytical) value of the functional ($f(U) \approx 2.138$).

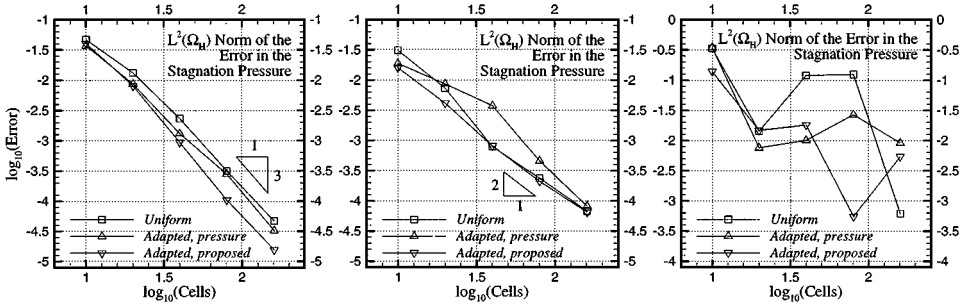

FIG. 10. Convergence in the $L^2(\Omega_H)$ norm of the error in the stagnation pressure. Results are presented for uniform grids, grids obtained using the adaptive strategy based on interpolation error in the computed pressure, and grids obtained using the proposed adaptive scheme. Left: subsonic flow; center: isentropic transonic flow; right: shocked flow.

is the product of the square of the cell size H_k and the absolute value of the second derivative of the pressure for cell k. A second-order, central difference was used to approximate the second derivative in (24).

The results in Figs. 7, 8, and 9 show that the accuracy of the functionals on the final adapted grids, before correction, are consistently better than their corresponding values on uniform grids of equal size. After application of the corrections, the adaptive results based on the proposed scheme become consistently more accurate than both the uniform grid results and the results obtained using the standard adaptive scheme. Note that the corrected functional values obtained using the standard scheme are generally less accurate than the corresponding uniform grid results. The disappointing performance of the interpolation-error indicator is likely due to the lack of a rigorous link between the second derivative in the pressure and the error in the computed functional [27].

Figure 10 shows the convergence in the $L^2(\Omega_H)$ norm of the error in the stagnation pressure where

$$\left\| p_o - p_o^H \right\|^2_{L^2(\Omega_H)} \equiv \int_0^L \left(p_o - p_o^H \right)^2 dx. \tag{25}$$

In this last expression, p_o is the exact (analytical) stagnation pressure and p_o^H is the finite volume approximation on Ω_H. For the purposes of evaluating the integral in (25), p_o^H is assumed to vary linearly within each cell. Figure 10 is provided as an example of how quantities other than the chosen functional converge using the proposed adaptive scheme.

The cell-size distributions corresponding to the final adapted grids using the proposed adaptive procedure are plotted in Fig. 11 on a logarithmic scale. For each flow regime, it is evident that the cell-size distributions corresponding to the 20-, 40-, 80-, and 160-cell grids are similar in shape; however, they become better defined, and appear to be converging to a fixed shape, as the total number of cells are increased. In each case, a clustering of cells occurs near the throat region. This is particularly true for the transonic flow cases, where the adjoint variables exhibit a singularity. In the shocked case, there is also a clustering of cells near the shock. In all cases, a coarsening of the grid occurs at the ends of the nozzle where the cross-sectional areas are constant. This effect becomes more pronounced as the total number of cells is increased. Lastly, there is a slight clustering of cells in the two regions of the nozzle where the constant-area portions of the duct join with the varying-area section. At these two points, the second derivative of the nozzle area is discontinuous.

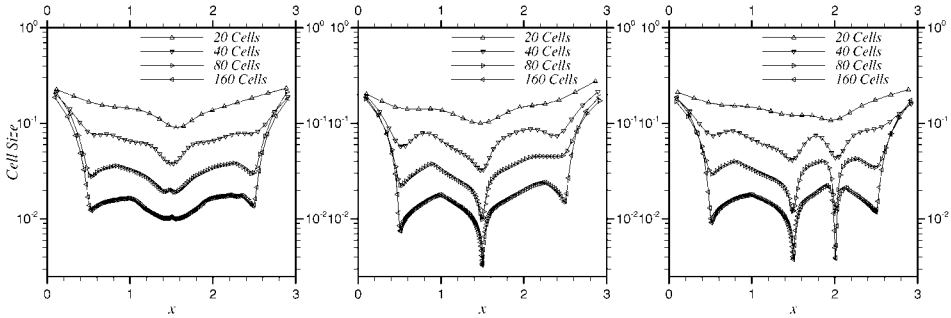

FIG. 11. Converged cell-size distributions (final adapted grids) after application of the proposed adaptive strategy to each of the quasi-1D Euler test cases considered. The total number of cells was fixed during each adaptive run. Left: subsonic flow; center: isentropic transonic flow; right: shocked flow.

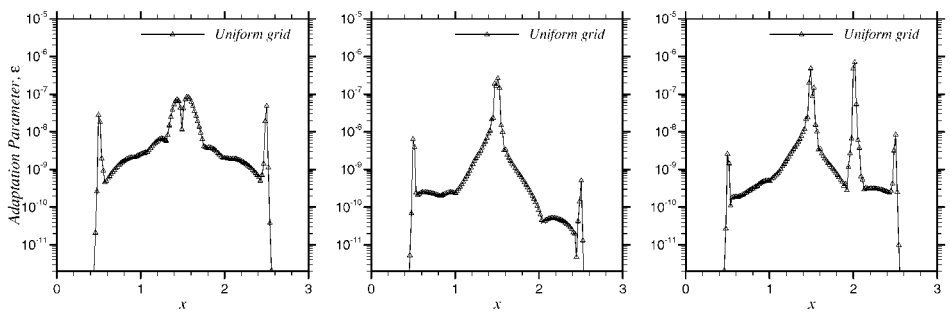

FIG. 12. Distributions of the adaptation parameter ε (corresponding to the proposed adaptive strategy) on a uniform, 160-cell grid for each of the quasi-1D Euler test cases considered. The adaptive algorithm strives to equidistribute the value of ε over the entire domain, where ε is given by (22). Left: subsonic flow; center: isentropic transonic flow; right: shocked flow.

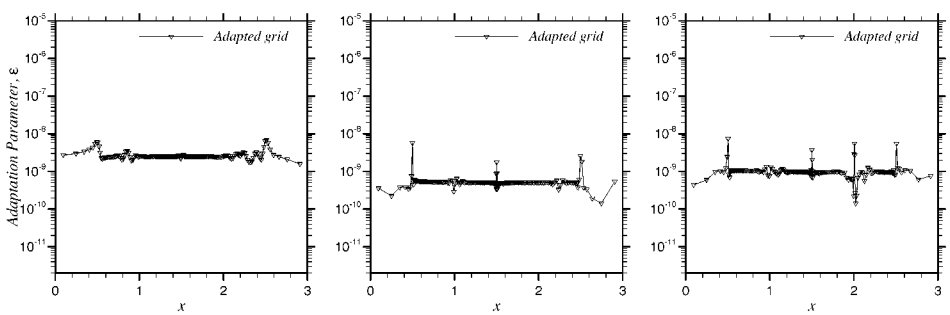

FIG. 13. Distributions of the adaptation parameter ε (corresponding to the proposed adaptive strategy) on the final, adapted, 160-cell grid for each of the quasi-1D Euler test cases considered. The adaptive algorithm strives to equidistribute the value of ε over the entire domain, where ε is given by (22). Left: subsonic flow; center: isentropic transonic flow; right: shocked flow.

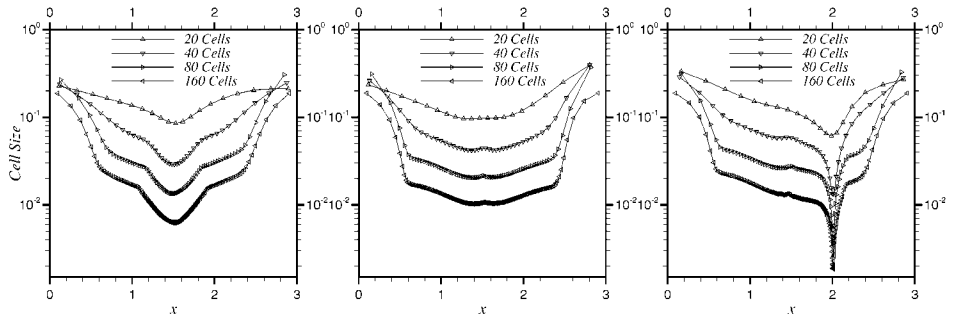

FIG. 14. Converged cell-size distributions (final adapted grids) after application of a standard adaptive scheme (based on the interpolation error in the computed pressure) to each of the quasi-1D Euler test cases considered. The total number of cells was fixed during each adaptive run. Left: subsonic flow; center: isentropic transonic flow; right: shocked flow.

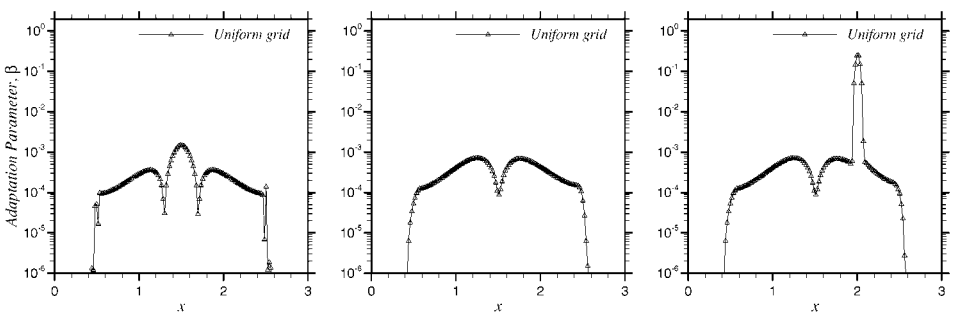

FIG. 15. Distributions of the adaptation parameter β (corresponding to a standard adaptive scheme based on the interpolation error in the computed pressure) on a uniform, 160-cell grid for each of the quasi-1D Euler test cases considered. The adaptive algorithm strives to equidistribute the value of β over the entire domain, where β is given by (24). Left: subsonic flow; center: isentropic transonic flow; right: shocked flow.

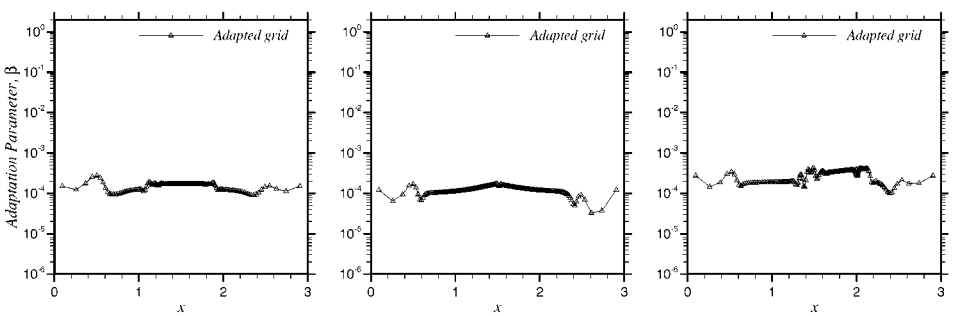

FIG. 16. Distributions of the adaptation parameter β (corresponding to a standard adaptive scheme based on the interpolation error in the computed pressure) on the final, adapted, 160-cell grid for each of the quasi-1D Euler test cases considered. The adaptive algorithm strives to equidistribute the value of β over the entire domain, where β is given by (24). Left: subsonic flow; center: isentropic transonic flow; right: shocked flow.

Figures 12 and 13 compare distributions of the adaptation parameter ε on uniform and adapted grids, respectively, for each of the test cases considered. The total number of cells was fixed at 160 during each adaptive run. As discussed in the previous section, the proposed adaptive algorithm strives to equidistribute the value of ε over the entire domain, where ε is given by (22). It is evident from each of the plots in Fig. 13 that ε was effectively equidistributed at the end of each adaptive run. It is interesting to note that the shapes of the distributions of ε on the uniform grids are similar to the shapes of the corresponding cell-size distributions of the final adapted grids (Fig. 11) after reflection of these curves 180° about the horizontal.

Figure 14 shows the cell-size distributions corresponding to the final adapted grids using the interpolation-error indicator to drive the adaptive process. In the shocked flow case, the indicator clusters cells near the shock, as expected. In contrast to the cell sizes in Fig. 11 (obtained using the proposed adaptive procedure), the interpolation-error indicator did not cluster cells near the throat in the transonic flow cases. Furthermore, it did not cluster cells near the points of discontinuous nozzle-area curvature. Underresolving the grid in these regions appears to have been the cause of the degraded accuracy in the predicted functional even when compared to the uniform grid results.

Figures 15 and 16 compare distributions of the adaptation parameter β on uniform and adapted grids, respectively, for each of the test cases considered.

The adaptive results presented in this section demonstrate that additional improvements in the accuracy of the functional can be achieved by applying the proposed adaptive strategy in conjunction with the error estimation procedure outlined in Section 2. It is anticipated, however, that the full potential of grid adaptivity will not be realized until the procedure is applied to multidimensional problems.

5. CONCLUSION

In this paper, an error estimation and grid adaptive strategy, based on a discrete adjoint formulation, was presented for improving the accuracy of specified integral outputs (functionals) from numerical solutions of partial differential equations. There are two stages to the error estimation procedure. The first stage involves estimating the error in the functional with respect to its value on a uniformly finer grid. The second stage involves a multilevel extrapolation process whereby the exact value of the functional is estimated. The main objective of the proposed adaptive procedure is to optimize the computational grid with respect to maximizing the quality of the aforementioned error estimation procedure. It was also shown that certain nonlinear contributions to the error can be reduced by the adaptive process. Numerical results were presented for the quasi-1D Euler equations. Both isentropic and shocked flows were considered. The error estimation procedure, applied on uniformly spaced grids, approximately doubled the accuracy of the computed functionals. Further improvements in accuracy were realized when the error estimation/correction procedure was applied in conjunction with the proposed adaptive strategy. A standard adaptive method, driven by a measure of the interpolation error in the computed pressure, was implemented and results were compared with those obtained from the proposed adaptive strategy. Adapting based on the interpolation error consistently yielded less accurate results. This is attributed to the lack of a rigorous link between the second derivative in the pressure and the error in the computed functional [27].

Finally, we note that grid adaptation for one-dimensional problems is seldom used in practice. It was employed in this paper to demonstrate the error estimation/grid adaptive concept in a relatively simple manner. It is expected that the adaptive strategy will play a far more important role in multidimensional problems. This is where the full potential of an adjoint-based adaptive strategy can be realized. In particular, if the problems under consideration involve multiple scales and isolated flow features such as shocks, wakes, and/or boundary layers, it is not always clear which parts of the computational grid should be refined to enhance the accuracy of the functional while maintaining computational efficiency. The main benefit of a well-resolved adjoint solution is that it will quantify the extent to which residual errors in the primal variables, at specific locations in the domain, affect the cumulative error in the functional. In theory, this will be the case regardless of the complexity or dimensionality of the flow problem under consideration. In practice, however, there are still several issues that need to be addressed upon extension of the proposed procedure to multiple dimensions. Among these issues are the difficulties associated with multidimensional interpolation and the definition of appropriate reconstruction operators, especially on unstructured grids. There is also the whole topic of anisotropic grid adaptation, which is particularly important for viscous flow computations. For such problems, the adaptive criteria will need to incorporate directional information to account for dramatic changes in length scales and in the types of transport phenomena (advection versus diffusion) occurring in various portions of the domain. Initial efforts to apply the procedure to 2-D inviscid and viscous transonic flows are currently underway [26].

APPENDIX

A.1. *Error Analysis*

In this section, we consider nonlinear contributions to the error in the functional estimate given by (6). We also revisit some of the developments of Section 4.1 and derive an explicit expression for the duality gap D.

The exact, truncated, second-order, Taylor series expansion of $f_h(U_h)$ about the coarse mesh solution can be written as

$$f_h(U_h) = f_h\big(U_h^H\big) + \left.\frac{\partial f_h}{\partial U_h}\right|_{U_h^H}\big(U_h - U_h^H\big) + \frac{1}{2}\big(U_h - U_h^H\big)^T \left.\frac{\partial^2 f_h}{\partial U_h^2}\right|_{U_h^\delta}\big(U_h - U_h^H\big), \quad \text{(i)}$$

where $h \le \delta \le H$. In this expression, $[\partial^2 f_h/\partial U_h^2]|_{U_h^\delta}$ is the Hessian matrix of second derivatives evaluated at U_h^δ. The vector U_h^δ represents the mapping onto Ω_h of the solution U_δ, corresponding to a mesh[3] Ω_δ, which is embedded within Ω_H, with average element (or cell) size δ.

Similarly, the residual operator $R_h(U_h)$ can be expanded as

$$R_h(U_h) = R_h\big(U_h^H\big) + \left.\frac{\partial R_h}{\partial U_h}\right|_{U_h^H}\big(U_h - U_h^H\big) + W, \quad \text{(ii)}$$

[3] Note that a mesh characterized by δ and embedded within Ω_H can only be associated with a rational value of δ/h. In general, the value of δ/h in (i) will be nonrational. Strictly, the results of this section do not require that δ be associated with a physical mesh and hence take on discrete values. Instead, δ should be regarded here as a continuous variable.

where

$$(W)_j = \frac{1}{2}\left(U_h - U_h^H\right)^T \left.\frac{\partial^2 (R_h)_j}{\partial U_h^2}\right|_{U_h^{\delta'}} \left(U_h - U_h^H\right), \tag{iii}$$

for each component j of the vector W. The term $[\partial^2 (R_h)_j / \partial U_h^2]|_{U_h^{\delta'}}$ represents the Hessian of the jth component of the residual vector, evaluated at $U_h^{\delta'}$. Furthermore, $h \le \delta' \le H$, and $U_h^{\delta'}$ is defined in the same manner as U_h^{δ} was above.

From (ii), one can symbolically obtain the solution error as

$$\left(U_h - U_h^H\right) = -\left.\frac{\partial R_h}{\partial U_h}\right|_{U_h^H}^{-1} \left(R_h\left(U_h^H\right) + W\right). \tag{iv}$$

Using (i), (iv), and the definition of the fine-mesh adjoint given by (7), we arrive at the following expression for the error in the computable correction:

$$\begin{aligned} f_h\left(U_h^H\right) - f_h(U_h) = {} & \underbrace{\left(L_h^H \Psi_H\right)^T R_h\left(U_h^H\right)}_{\text{Computable correction}} + \underbrace{\left(\Psi_h|_{U_h^H} - L_h^H \Psi_H\right)^T R_h\left(U_h^H\right)}_{\text{Error neglecting nonlinear effects}} \\ & + \underbrace{\Psi_h\big|_{U_h^H}^T W - \frac{1}{2}\left(U_h - U_h^H\right)^T \left.\frac{\partial^2 f_h}{\partial U_h^2}\right|_{U_h^{\delta}} \left(U_h - U_h^H\right)}_{\text{Error due to nonlinear effects}}. \end{aligned} \tag{v}$$

Finally, transposing (18), right-multiplying the result by $[\partial R_h / \partial U_h|_{U_h^H}]^{-1} R_h(U_h^H)$, and using (iv) leads to

$$\begin{aligned} \left(\Psi_h|_{U_h^H} - L_h^H \Psi_H\right)^T R_h\left(U_h^H\right) &= -R_h^\Psi \left(L_h^H \Psi_H\right)^T \left[\left.\frac{\partial R_h}{\partial U_h}\right|_{U_h^H}\right]^{-1} R_h\left(U_h^H\right) \\ &= R_h^\Psi \left(L_h^H \Psi_H\right)^T \left[\left(U_h - U_h^H\right) + \left[\left.\frac{\partial R_h}{\partial U_h}\right|_{U_h^H}\right]^{-1} W\right] \\ &= R_h^\Psi \left(L_h^H \Psi_H\right)^T \left(U_h - U_h^H\right) - \left(\Psi_h|_{U_h^H} - L_h^H \Psi_H\right)^T W, \end{aligned} \tag{vi}$$

from which the duality gap D is obtained as

$$\begin{aligned} D &\equiv \left(\Psi_h|_{U_h^H} - L_h^H \Psi_H\right)^T R_h\left(U_h^H\right) - \left\{R_h^\Psi \left(L_h^H \Psi_H\right)\right\}^T \left(U_h - U_h^H\right) \\ &= -\left(\Psi_h|_{U_h^H} - L_h^H \Psi_H\right)^T W. \end{aligned} \tag{vii}$$

ACKNOWLEDGMENTS

The authors gratefully acknowledge the support of the National Science Foundation, The Boeing Company, and NASA Langley during various stages of this research. We wish to thank Professor Mike Giles of the Oxford Computing Laboratory for several useful comments regarding the error estimation procedure proposed in this paper. The first author also acknowledges FCAR (Fonds pour la Formation de Chercheurs et l'Aide à la Recherche) for its support.

REFERENCES

1. M. Ainsworth and J. T. Oden, A posteriori error estimation in finite element analysis, *Comput. Meth. Appl. Mech. Eng.* **142**, 1 (1997).
2. I. Babuška and A. Miller, The post-processing approach in the finite element method—Part 1: Calculation of displacements, stresses and other higher order derivatives of the displacements, *Int. J. Numer. Meth. Eng.* **20**, 1085 (1984).
3. T. J. Baker, Mesh adaptation strategies for problems in fluid dynamics, *Finite Elements Anal. Design*. **25**, 243 (1997).
4. R. Becker and R. Rannacher, *Weighted A Posteriori Error Control in Finite Element Methods*, Technical report, preprint No. 96-1, Universitat Heidelberg (1994).
5. M. Braack and R. Rannacher, Adaptive Finite Element Methods for Low-Mach-Number Flows with Chemical Reactions, in *30th Computational Fluid Dynamics*, von Karman Institute Lecture Series 1999–03 (von Karman Institute for Fluid Dynamics, Rhode-Saint-Genese, 1999).
6. J. Elliot and J. Peraire, *Aerodynamic Optimization on Unstructured Meshes with Viscous Effects*, AIAA Pap. 97-1849 (1997).
7. M. B. Giles, Analysis of the accuracy of shock-capturing in the steady quasi-1D Euler equations, *Comput. Fluid Dyn. J.* **5**, 247 (1996).
8. M. B. Giles, On adjoint equations for error analysis and optimal grid adaptation in CFD, in *Computing the Future II: Advances and Prospects in Computational Aerodynamics*, edited by M. Hafez and D. A. Caughey (Wiley, New York, 1998).
9. M. B. Giles and N. A. Pierce, *Adjoint Equations in CFD: Duality, Boundary Conditions and Solution Behavior*, AIAA Pap. 97-1850 (1997).
10. J. F. Hétu and D. H. Pelletier, Fast, adaptive finite element scheme for viscous incompressible flows, *AIAA J.* **30**(11), 2677 (1992).
11. C. Hirsch, *Numerical Computation of Internal and External Flows. Computational Methods for Inviscid and Viscous Flows* (Wiley, Chichester, England, 1992), Vol. 2.
12. A. Jameson, N. A. Pierce, and L. Martinelli, *Optimum Aerodynamic Design Using the Navier–Stokes Equations*, AIAA Pap. 97-0101 (1997).
13. C. Johnson and R. Rannacher, *On Error Control in CFD*, Technical report, preprint No. 94-13, Universitat Heidelberg (1994).
14. L. Machiels, J. Peraire, and A. T. Patera, A posteriori finite element bounds for the incompressible Navier–Stokes equations: Application to a natural convection problem, submitted for publication.
15. E. J. Nielsen and W. K. Anderson, *Aerodynamic Design Optimization on Unstructured Meshes Using the Navier–Stokes Equations*, AIAA Pap. 98-4809 (1998).
16. E. Onate and G. Bugeda, Mesh optimality criteria for adaptive finite element computations, in *The Mathematics of Finite Elements and Applications*, edited by J. R. Whiteman (Wiley Chichester, England, 1994), p. 121.
17. J. Peraire and A. T. Patera, Asymptotic a posteriori finite element bounds for the outputs of noncoercive problems: The Helmholtz and Burgers equations, *Comput. Meth. Appl. Mech. Eng.* **171**, 77 (1999).
18. J. Peraire, M. Vahdati, K. Morgan, and O. C. Zienkiewicz, Adaptive remeshing for compressible flow computations, *J. Comput. Phys.* **72**, 449 (1987).
19. N. A. Pierce and M. B. Giles, Adjoint recovery of superconvergent functionals from PDE approximations, *SIAM Rev*. **42**, 247 (2000).
20. L. F. Richardson, The approximate arithmetic solution by finite differences of physical problems involving differential equations with application to stresses in a masonry dam, *Trans. Roy. Soc. London Ser. A* **210**, 307 (1910).
21. L. F. Richardson, The deferred approach to the limit, *Trans. Roy. Soc. London Ser. A* **226**, 299 (1927).
22. P. L. Roe, Approximate Riemann solvers, parameter vectors, and difference schemes, *J. Comput. Phys.* **43**, 357 (1981).
23. A. H. Shapiro, *The Dynamics and Thermodynamics of Compressible Fluid Flow* (Ronald Press Company, New York, 1953), Vol. 1.

24. G. D. van Albada, B. van Leer, and W. W. Roberts, A comparative study of computational methods in cosmic gas dynamics, *Astron. Astrophys*. **108**, 95 (1982).
25. B. van Leer, Towards the ultimate conservative difference scheme. V. A second order sequel to Godunov's method, *J. Comput. Phys.* **32**, 101 (1979).
26. D. A. Venditti and D. L. Darmofal, *Grid Adaptation for Functional Outputs of 2-D Compressible Flow Simulations*, AIAA Pap. 2000-2244 (2000).
27. G. P. Warren, W. K. Anderson, J. T. Thomas, and S. L. Krist, *Grid Convergence for Adaptive Methods*, AIAA Pap. 91-1592 (1991).
28. J. Wu, J. Z. Zhu, J. Szmelter, and O. C. Zienkiewicz, Error estimation and adaptivity in Navier–Stokes incompressible flows, *Comput. Mech.* **6**, 259 (1990).
29. O. C. Zienkiewicz and J. Z. Zhu, A simple error estimation and adaptive procedure for practical engineering analysis, *Int. J. Numer. Meth. Eng.* **24**, 337 (1987).
30. O. C. Zienkiewicz and J. Z. Zhu, The superconvergent patch recovery and a posteriori error estimates. Part 1: The recovery technique, *Int. J. Numer. Meth. Eng.* **33**, 1331 (1992).